Compatibility between polymethacrylate-based extreme ultraviolet resists and TiO$_2$ area-selective deposition

Rachel A. Nye,[a,b,c] Kaat Van Dongen,[a,b] Hironori Oka,[d] Danilo De Simone,[a] Gregory N. Parsons,[c] and Annelies Delabie[a,b,*]

^{a}IMEC, Leuven, Belgium
^{b}KU Leuven (University of Leuven), Leuven, Belgium
^{c}North Carolina State University, Department of Chemical and Biomolecular Engineering, Raleigh, North Carolina, United States
^{d}FUJIFILM Corporation Electronic Materials Research Laboratories, Yoshida-Cho, Japan

Abstract

Background: Extreme ultraviolet (EUV) lithography is crucial to achieving smaller device sizes for next-generation technology, although organic resists face substantial challenges, such as low etch resistance, which limit the resolution of smaller features.

Aim: Evaluate the potential for area-selective deposition (ASD) to improve EUV pattern resolution (e.g., by increasing etch resistance).

Approach: We evaluate thermal compatibility, atomic layer deposition growth rate, and selectivity for TiO$_2$ ASD on various organic EUV resist materials using water contact angle, Rutherford backscattering spectrometry, and X-ray photoelectron spectroscopy. The effects of photo-acid generator (PAG) and EUV exposure on polymer properties and selectivity are considered.

Results: The organic resist materials studied demonstrate thermal compatibility with TiO$_2$ ALD (125°C for 60 min). The TiO$_2$ ALD process from TiCl$_4$ and H$_2$O proceeds readily on poly(*tert*-butyl methacrylate), poly(p-hydroxystyrene), and poly(p-hydroxystyrene-random-methacrylic acid) polymers, with and without PAG incorporation, in either the as-formed or EUV exposed state. However, TiO$_2$ is inhibited on poly(cyclohexyl methacrylate).

Conclusions: We demonstrate that as-formed EUV resists can serve as either the growth or nongrowth surface during TiO$_2$ ASD, thereby enabling resist hardening and tone inversion applications, respectively. These results serve as a basis for further ASD studies on EUV resist materials to improve pattern resolution in next-generation devices.

© 2022 Society of Photo-Optical Instrumentation Engineers (SPIE) [DOI: 10.1117/1.JMM.21.4.041407]

Keywords: extreme ultraviolet lithography; photoresist; area-selective deposition; atomic layer deposition; TiO$_2$; polymethacrylate.

1 Introduction

As semiconductor manufacturing approaches next-generation technology nodes (<7 nm), the need for high-NA extreme ultraviolet (EUV) lithography is becoming increasingly apparent.[1] One of the biggest obstacles is the development of resist materials that can simultaneously improve pattern resolution, line-edge roughness (LER), and sensitivity, i.e., the RLS tradeoff.[2–4] Commonly used chemically amplified resists (CARs) could benefit from the addition of a material with higher etch resistance to improve resolution and LER. Another potential method to improve CAR performance is tone inversion, for example inverting the pattern from a positive

Fig. 1 (a) Schematic of EUV lithographic patterning (in this case on positive tone resist) in conjunction with ASD for resist hardening or tone inversion applications. (b) Schematic of the experimental procedure used herein.

tone resist (which is typically easier to fabricate) to create a negative pattern from a higher etch resistance material (e.g., TiO_2).[4–6] One advancing technique that has the potential to improve patterning processes in the aforementioned ways and thus greatly improve EUV lithography performance is area-selective deposition (ASD).[7–9]

ASD is a bottom-up nanopatterning technique that exploits chemical differences on a surface to deposit material in one region without depositing in an adjacent region.[7,8,10] This is typically achieved with chemical vapor deposition (CVD) or atomic and molecular layer deposition (ALD/MLD), the latter of which relies on self-limiting vapor-solid surface reactions to deposit material with nanoscale thickness control.[8,10–13] Thus, an area-selective ALD/MLD process is highly controllable in terms of deposited layer thickness and conformality.[13] Combining ASD with EUV lithography could reduce edge placement error, reduce resist thickness requirements, and provide a means to prevent or repair line breaks and decorate defects.[14–16] Thus, area-selective ALD shows promise for depositing etch-resistant layers on EUV resists to enable tone inversion or resist hardening to improve pattern resolution, as shown schematically in Fig. 1.[14,17–19] However, as ASD processes are extremely surface-sensitive, integrating ASD with resist materials requires consideration of every resist component, including the polymer backbone, protecting groups, photo decomposable base, quencher, and number and type of PAGs.

TiO_2 is one ASD-compatible material of particular interest for its high etch resistance, chemical stability, and compatibility with low-temperature ($\sim$100°C) processing.[20,21] This film has high reactivity with OH surface groups, such as those expected on exposed resist surfaces. Furthermore, TiO_2 ALD has demonstrated excellent selectivity in many ASD processes, including on substrates such as amorphous carbon, H-terminated Si, SiO_2, TiO_2, Ru, and TiN.[15,22,23] Despite these benefits, studies of TiO_2 on EUV resist materials so far focus mainly on layers thicker than 100 nm, while much thinner materials are needed for patterning with high NA EUV lithography.[9,24]

In this work, we investigate the compatibility between TiO_2 ALD and $\sim$30 nm thin EUV resist materials for potential use in ASD of a resist-hardening or tone-inverting layer. We first evaluate the thermal compatibility of $\sim$30 nm organic photoresist materials with the TiO_2 ALD
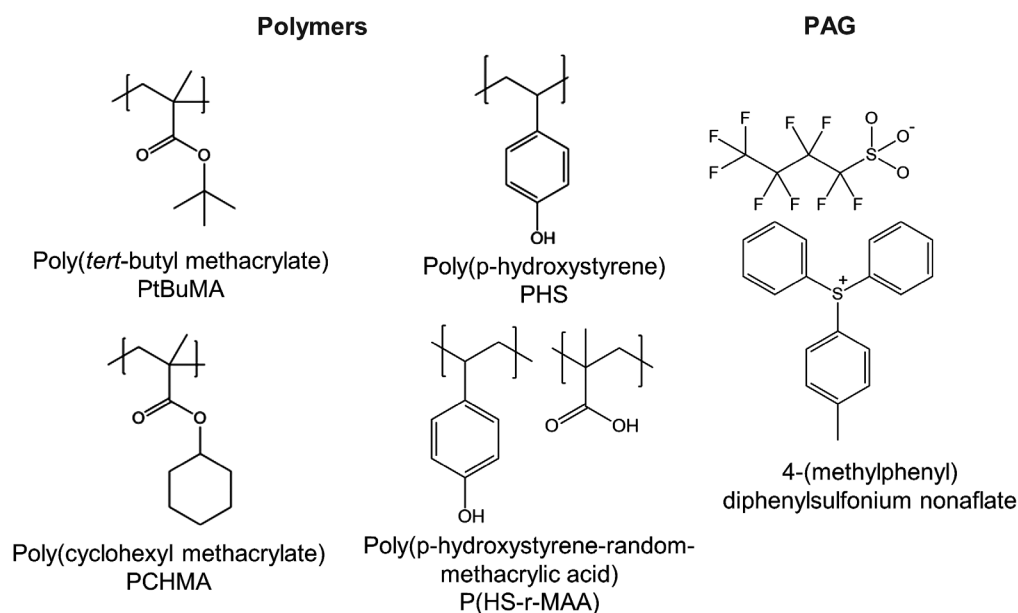
temperature window. We systematically consider the effects of resist additives (e.g., PAG and EUV exposure) on surface hydrophobicity and roughness at ALD temperatures. Next, we determine the TiO_2 growth rate and $TiCl_4$ precursor reactivity on several resist materials, before and after EUV exposure, again discussing the impact of PAG and EUV exposure on ALD. Finally, we investigate how the polymer protecting group influences the TiO_2 growth rate and discuss potential applications for each resist material. We utilize this insight to identify relevant challenges and future directions to pave the way for effective collaborations between ASD and EUV lithography.

2 Experimental

The EUV resist materials used in this work are provided by Fujifilm and consist of organic polymers with methacrylate backbones and various protecting groups, as shown in Fig. 2. All CAR processing occurred on cleanroom compatible 300 mm wafer tools. We focus on poly(*tert*-butyl methacrylate) (PtBuMA), poly(p-hydroxystyrene) (PHS), poly(p-hydroxystyrene-random-methacrylic acid) (P(HS-r-MAA)), and poly(cyclohexyl methacrylate) (PCHMA). In some experiments, a photo-acid generator (PAG), 4-(methylphenyl) diphenylsulfonium nonaflate, is also incorporated into the polymers, with the PAG structure shown in Fig. 2. Starting on 300 mm Si wafers with thin SiO_2, the surface is first primed with hexamethyldisilazane (HMDS). The polymers of interest are spin-coated to ∼30 nm, then treated with a postapply bake (PAB) at 120°C for 90 s. In some experiments, the polymers are then exposed to 15 mJ/cm² EUV light and undergo a post exposure bake (PEB) at 120°C for 90 s in an ASML full-field NXE:3300B scanner. Five regions (∼2 cm × ∼3 cm) are exposed in a line across the center of the 300 mm wafer. Development is performed on the positive tone poly(p-hydroxystyrene-random-*tert*-butyl methacrylate) copolymer (P(HS-r-tBuMA)) using 0.26 N tetramethylammonium hydroxide (TMAH) solution. We note that the CARs selected here have generally well-understood mechanisms after EUV exposure, which lead to changes in surface -OH site density and are expected to cause differences in growth rate on different surfaces.

TiO_2 is deposited via ALD (Polygon 8300 EmerALD) with $TiCl_4$ and H_2O at 125°C and 5 Torr nitrogen (N_2) on blanket exposed or unexposed regions of the resist materials using a recipe that demonstrates good saturation on SiO_2 surfaces, resulting in a growth rate of ∼0.037 nm/cycle on SiO_2.[19,22,23] A summary of the experimental procedure is included in Fig. 1(b).

Polymer materials are characterized using various techniques. Fourier transform infrared spectroscopy (FTIR) is performed with a Nicolet 6700 Spectrometer from Thermoelectron

Polymers

Poly(*tert*-butyl methacrylate)
PtBuMA

Poly(p-hydroxystyrene)
PHS

Poly(cyclohexyl methacrylate)
PCHMA

Poly(p-hydroxystyrene-random-methacrylic acid)
P(HS-r-MAA)

PAG

4-(methylphenyl) diphenylsulfonium nonaflate

Fig. 2 Structures for each polymer and PAG utilized in this work.

Corporation using a range of 400 to 4000 cm^{-1} and resolution of 0.2 cm^{-1} to determine resist composition. Water contact angle (WCA) measurements are used to measure surface hydrophobicity and are performed on a Dataphysics OCAH 230 tool using 1 μL droplets of deionized water, with the average value of five measurements reported for each sample. RMS roughness is measured with atomic force microscopy (AFM) on a Bruker dimension edge instrument in tapping mode with ScanAsyst and a 300 kHz tip. Polymer film thickness is measured using spectroscopic ellipsometry on a KLA Tencor F5-SCD instrument. X-ray photoelectron spectroscopy (XPS) is performed on a Thermo Scientific Theta 300 tool to measure surface elemental composition. The source is a 1486.6 eV monochromatized Al Kα X-ray source and the spot size is 400 μm. The XPS spectra are corrected to the C 1s peak at a binding energy of 284.8 eV. The Ti content on the polymers is quantified using Rutherford backscattering spectrometry (RBS) with a 1.523 MeV He$^+$ ion beam, which is then converted to an equivalent TiO$_2$ film thickness using a TiO$_2$ density of 3.72 g cm^{-3}.

3 Results and Discussion

3.1 *EUV Polymer Resist Characterization*

To demonstrate the ability of these polymer materials to function as resist systems, we selected PtBuMA as a model system and analyzed it with FTIR in its as-spin-coated form and after EUV exposure and PEB, with results shown in Fig. 3. The exposure is performed with 15 mJ/cm^2 EUV light, producing a pattern of five ~2 $\times$ 3 cm exposed regions along the centerline of the 300 mm wafer. Figure 3(a) shows the expected structure of the PtBuMA resist before and after EUV exposure and PEB, where the PAG is thermally activated during PEB to cleave the C-O bond linking the ester to the tBu protecting group, thereby converting the methyl-terminated surface (hydrophobic) to a hydroxyl-terminated surface (hydrophilic).[1,24] This transition is confirmed with FTIR results in Fig. 3(b). Specifically, we note the conversion of the CH$_3$ stretching peak (~3000 cm^{-1}) for the unexposed PtBuMA polymers (both with and without PAG) to an OH stretching peak (~2800 to 3300) after exposure and PEB.[24] Additionally, the C(CH$_3$) stretch at ~1370 cm^{-1} disappears after exposure, and the peak at ~1720 cm^{-1} before exposure (COOR) is shifted to ~1700 cm^{-1} after exposure (COOH).[24] This change during exposure and PEB is expected to cause a difference in the rate of TiO$_2$ nucleation during ASD, thus enabling faster growth on the EUV exposed, hydrophilic surface while inhibiting growth on the unexposed, hydrophobic surface.[8,15,19]

In addition to the PtBuMA model system, we also use P(HS-r-tBuMA) copolymer as a model system to evaluate development with TMAH. After EUV exposure and PEB, the copolymer film thickness is measured with ellipsometry, with results shown in Fig. 4. Then, after development, the copolymer is analyzed with WCA and XPS, with results shown in Fig. 5 and Table 1.
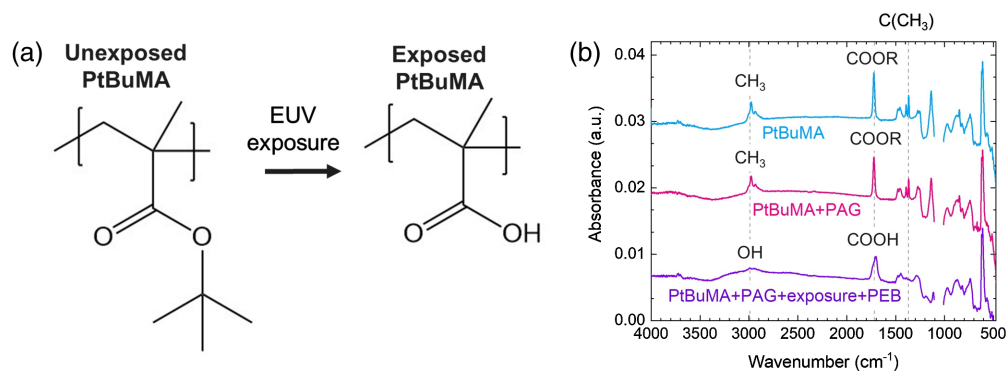
Fig. 3 (a) Structure of the PtBuMA polymer before and after EUV exposure, showing conversion from tBu to OH groups. (b) FTIR spectra of PtBuMA only (blue), PtBuMA with PAG (pink), and PtBuMA with PAG after EUV exposure and PEB (purple). Relevant peaks are indicated. Si-O peak at ~1100 cm^{-1} is omitted for clarity.
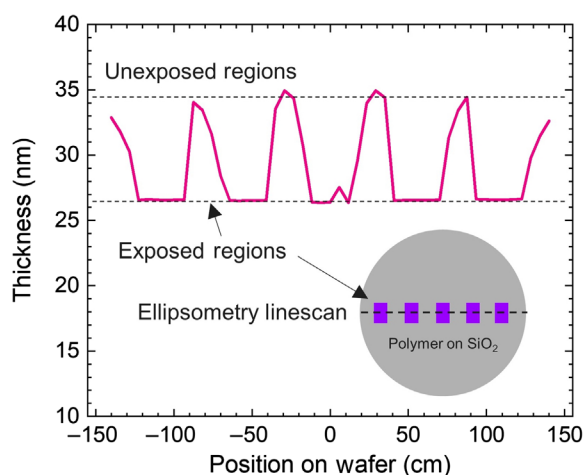
Fig. 4 Ellipsometry linescan of P(HS-r-tBuMA) polymer with PAG patterned with five ~2 cm wide regions of EUV exposed resist separated by unexposed resist.
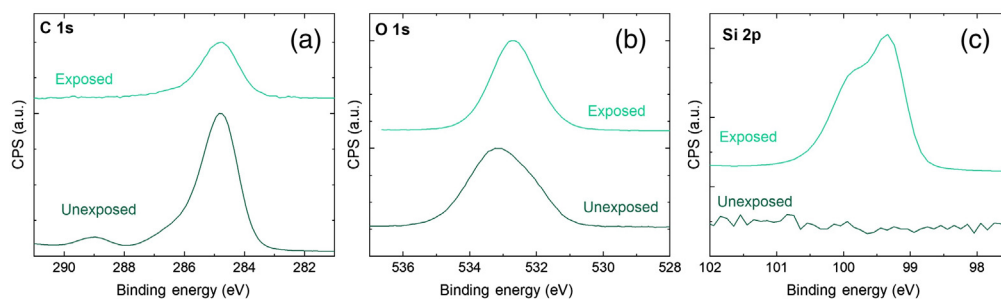
Fig. 5 XPS high resolution scans for (a) C 1s, (b) O 1s, and (c) Si 2p on P(HS-r-tBuMA) + PAG after development on both EUV exposed and unexposed regions of resist.

Table 1 WCA and XPS results on P(HS-r-tBuMA) with PAG before and after development for both EUV exposed and unexposed resist regions.

			XPS atomic concentration		
P(HS-r-tBuMA) + PAG		WCA (deg)	C 1s	O 1s	Si 2p
Unexposed	Before development	72 ± 4	—	—	—
	After development	73 ± 4	81.21	17.11	0.17
Exposed	Before development	61 ± 3	—	—	—
	After development	45 ± 3	12.69	28.84	58.26

Figure 4 shows thickness results from an ellipsometry linescan across the center of the EUV-exposed P(HS-r-tBuMA) polymer film. The film thickness is fairly consistent within each region, where the exposed regions are thinner than the unexposed regions (~27 nm compared with ~35 nm, respectively), consistent with the removal of the bulky tBu protecting groups from the exposed regions.

Figure 5 shows high-resolution XPS scans of the C 1s, O 1s, and Si 2p regions for EUV exposed and unexposed P(HS-r-tBuMA) resist after development. Corresponding atomic concentrations and WCA measurements are summarized in Table 1. The C 1s signal [Fig. 5(a)] at 289 eV, corresponding to the O─C═O bond in the methacrylate polymer backbone, is present only in the unexposed resist. The O 1s signal [Fig. 5(b)] is similar for developed resist in both

exposed and unexposed regions, whereas the Si 2p signal [Fig. 5(c)] is observed only on the exposed resist. Atomic concentrations from XPS listed in Table 1 reveal a substantial decrease in carbon and increase in silicon signals after the development of the exposed resist compared with the unexposed resist. We note the presence of some F in each sample (not shown in Table 1), attributed to small amounts of contamination during resist processing. The WCA on the unexposed resist does not change significantly from ~72 deg after development. However, after developing the EUV exposed resist, the WCA decreases from 61 deg (after EUV exposure) to 45 deg (after development), which is close to the hydrophilic WCA expected for the underlying SiO_2 substrate (~25 deg). These results are consistent with removal of the exposed resist after development without significantly affecting the unexposed regions.

3.2 Resist Thermal Compatibility with ALD

Next, we evaluate the PtBuMA, PHS, and P(HS-r-MAA) polymer surface properties before and after heating to typical ALD temperatures (90°C to 180°C) to determine polymer thermal compatibility. The spin-coated polymers are examined using three conditions: (1) without PAG, (2) with PAG, and (3) with PAG after EUV exposure and PEB. To simulate an ALD process, the polymers are placed in an oven for 60 min at various temperatures between 90°C and 180°C under a lab air ambient environment. The annealed surfaces are analyzed using WCA to measure surface hydrophobicity, AFM to measure surface roughness, and XPS to measure surface composition, with results shown in Figs. 6–8 and Table 2. Here, we consider the polymers to be
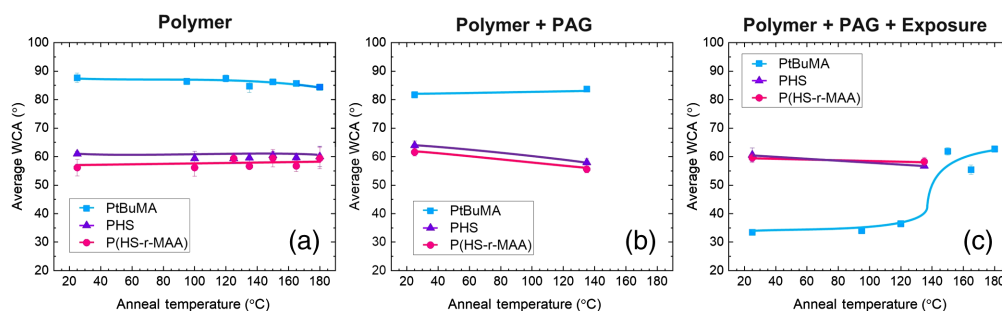
Fig. 6 Water contact angle measurements for PtBuMA (blue squares), PHS (purple triangles), and P(HS-r-MAA) (pink circles) as a function of anneal temperature for samples of (a) polymers without PAG, (b) polymers with PAG, and (c) polymers with PAG after EUV exposure and PEB. Lines are drawn as guides to the eye.
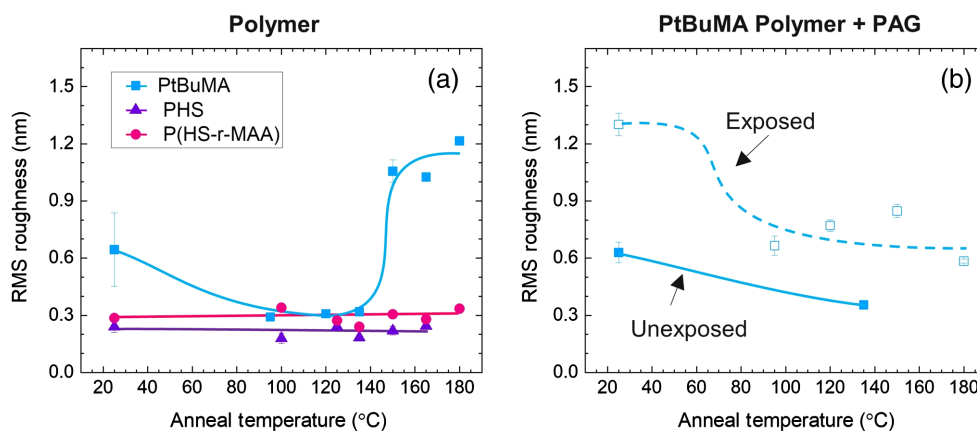
Fig. 7 RMS roughness measurements from AFM for PtBuMA (blue squares), PHS (purple triangles), and P(HS-r-MAA) (pink circles) as a function of anneal temperature for samples of (a) polymers without PAG and (b) PtBuMA with PAG before (filled shapes) and after (open shapes) EUV exposure and PEB. Lines are drawn as guides to the eye.
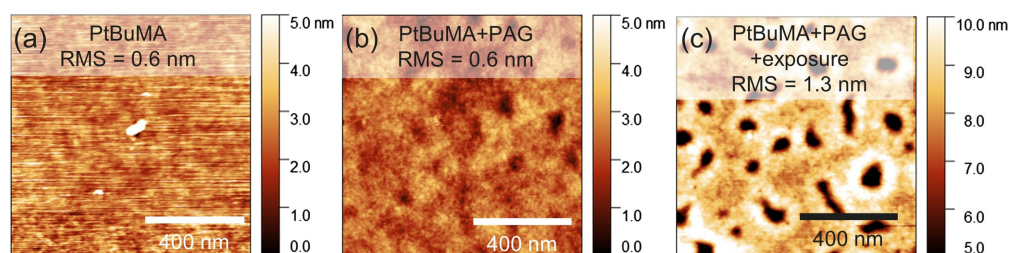
Fig. 8 Topographical images from AFM over $1\ \mu m \times 1\ \mu m$ areas for PtBuMA (a) without PAG, (b) with PAG, and (c) with PAG after EUV exposure and PEB. Note the *z*-scale increases from 5 nm in (a) and (b) to 10 nm in (c).

Table 2 XPS measurements for atomic concentrations of C, O, and Si on PtBuMA without PAG, with PAG, and with PAG after EUV exposure and PEB. Data are collected at an angle of 20 deg to the surface.

PtBuMA polymer	XPS atomic concentration		
	C 1s	O 1s	Si 2p
Polymer only	81.81	18.13	0.07
With PAG	82.14	17.35	0.51
With PAG after exposure	83.99	15.49	0.53

thermally stable if they undergo minimal changes to surface WCA and roughness after annealing.[19]

Figure 6 shows the WCA of each polymer under different conditions, demonstrating minimal changes in surface hydrophobicity up to at least ~135°C for all samples. As spin-coated, the methyl-terminated PtBuMA has the largest WCA (~88 deg), while the hydroxyl-terminated PHS and P(HS-r-MAA) polymers have a smaller contact angle of around 59 deg, as seen in Fig. 6(a). After incorporating the PAG [Fig. 6(b)], the WCA of PtBuMA decreases slightly (to ~82 deg), while the WCAs of PHS and P(HS-r-MAA) increase slightly (to ~63 deg). After exposing the polymers with PAG [Fig. 6(c)] to EUV light, the PtBuMA polymer with a cleavable protecting group (i.e., tBu) becomes more hydrophilic (WCA ~ 33 deg), while the WCAs of PHS and P(HS-r-MAA) (which do not have cleavable protecting groups) are maintained around 60 deg.

After annealing, we observe different trends in WCA for the different polymers. There is no change to the WCA of any polymer when annealing up to ~135°C, indicating thermal stability below this temperature. We note that this is the highest annealing temperature studied for some samples, as indicated in the Figure. A consistent WCA is also maintained up to 180°C annealing for PHS and P(HS-r-MAA) polymers without PAG [Fig. 6(a)]. However, when heating the PtBuMA polymer without PAG above 135°C, the WCA increases slightly [Fig. 6(a)], indicating some thermally-induced changes to the surface. Furthermore, after heating the EUV-exposed PtBuMA+PAG sample to ~150°C, the WCA increases dramatically from ~33 deg to ~60 deg, indicating poor thermal stability at this temperature. These differences in stability for different polymers and for EUV exposed versus unexposed resists highlight an important challenge in conducting ASD on EUV resists, as associated lithographic processing (e.g., addition of PAG, EUV exposure, etc.) may affect the resist surface properties relevant to ASD.

Figure 7 shows RMS surface roughness measured by AFM. For as spin-coated polymers without PAG [Fig. 7(a)], PtBuMA has a much larger surface roughness (~0.6 nm) compared with PHS or P(HS-r-MAA) (<0.3 nm). For PtBuMA, the RMS roughness does not change significantly after incorporating PAG, but increases substantially to ~1.3 nm after EUV exposure [Fig. 7(b)]. After annealing, the roughness of the hydroxyl-terminated polymers (PHS and P(HS-r-MAA)) does not change, consistent with WCA results in Fig. 6(a). In contrast, the roughness of

PtBuMA decreases significantly from 0.6 to ~0.3 nm after annealing at 95℃, but increases again to ~1.1 nm at 150℃ (consistent with the slight decrease in WCA observed in Fig. 6(a) at 150℃). A similar trend is observed for the PtBuMA polymer with PAG [Fig. 7(b)], where RMS roughness decreases from ~0.6 as spin-coated to ~0.3 nm after annealing at 135℃. However, the surface roughness of the EUV exposed PtBuMA+PAG sample [Fig. 7(b)] decreases to ~0.7 nm after annealing at temperatures between 95℃ and 180℃, despite a stable contact angle for the PtBuMA surfaces up to ~135℃ [Fig. 6(c)]. Based on these results, we select 125℃ to represent a reasonable processing temperature for TiO_2 ALD where minimal changes are apparent in WCA and surface roughness for as-deposited and annealed polymers.

The PtBuMA surface morphology is further investigated with AFM topographical scans over a 1 μm × 1 μm area, shown in Fig. 8. Without PAG, the surface is relatively smooth and homogeneous [Fig. 8(a)]. When incorporating the PAG into the polymer [Fig. 8(b)], some darker regions appear on the image, corresponding to holes in the surface, which are attributed to phase separation between the hydrophobic polymer and the PAG. After exposure [Fig. 8(c)], these darker regions have increased in frequency and intensity, indicating large craters across the polymer surface. These craters measure ~80 to 160 nm wide and 3 to 9 nm deep, which is close to the average exposed film thickness of ~11 nm for EUV exposed PtBuMA+PAG (according to ellipsometry). XPS data in Table 2 reveals an increase in Si concentration detected on samples with PAG (both before and after EUV exposure), providing further evidence that the craters formed on the exposed PtBuMA+PAG surface reach close to the underlying Si substrate. Consistent surface chemistry is critical for successful ASD, thus the phase separation indicated by AFM and XPS between PtBuMA and PAG could result in low selectivity. Future work should seek to reduce phase separation in resist materials, for example by utilizing copolymers or various protecting groups.

## 3.3 TiO_2 ALD on Exposed versus Unexposed Polymers

The TiO_2 ALD process has been well-established in literature on SiO_2,[15,22,23,25] although ALD on polymer surfaces is known to cause differences in growth behavior compared to metal oxide substrates, for example enabling subsurface precursor diffusion or additional water-uptake in the polymer before deposition.[9,26–29] The effects of water absorbed into the polymers before deposition could be mitigated with longer purge times or sample degas times before deposition. Therefore, we evaluate the effects of varying purge and degas time on the TiO_2 growth rate by depositing 100 cycles of TiO_2 on PtBuMA using a previously established ALD process with demonstrated saturation and plotting the measured Ti content from RBS as a function of process time.[22] From the Ti aerial density, the equivalent TiO_2 thickness is calculated using 3.72 g/cm^3 TiO_2 density. Results are shown in Figs. 9(a) and 9(b), respectively.

From Fig. 9, the Ti uptake after 100 cycles of TiO_2 ALD on PtBuMA using standard conditions of 6 s purges and 1 min degas is ~8.4 × 10^{15} Ti-at/cm^2. When increasing the purge time to 30 s [Fig. 9(a)], the Ti aerial density decreases only slightly (to ~7.9 × 10^{15} Ti-at/cm^2).
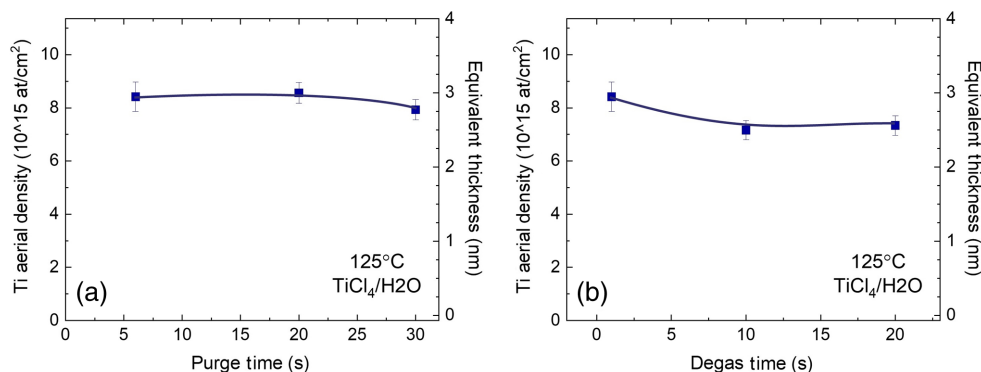
Fig. 9 RBS results for Ti content (left y-axis) and equivalent film thickness (right y-axis) after 100 cy TiO_2 ALD at 125°C on PtBuMA as a function of (a) purge time and (b) degas time.
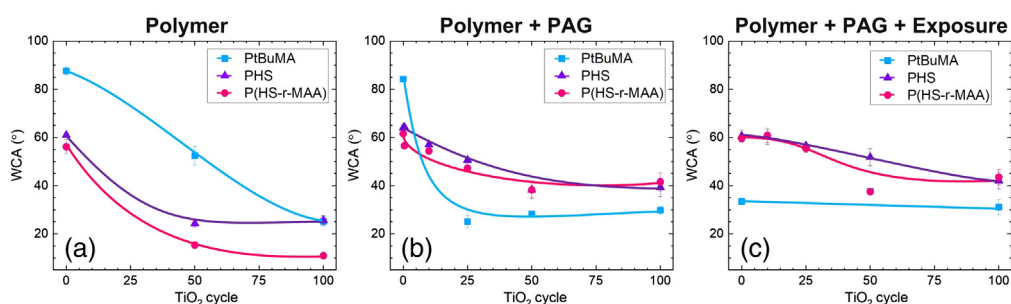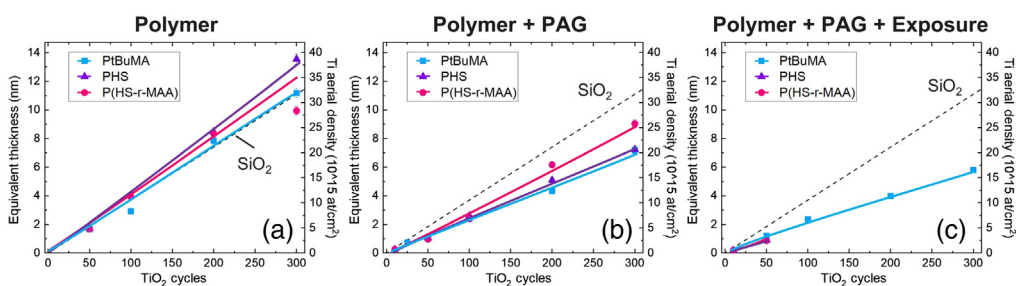
Fig. 10 WCA measurements after various cycles of TiO_2 ALD from $TiCl_4$ and H_2O at 125°C on PtBuMA (blue squares), PHS (purple triangles), and P(HS-r-MAA) (pink circles) for samples of (a) polymers without PAG, (b) polymers with PAG, and (c) polymers with PAG after EUV exposure and PEB. Lines are drawn as guides to the eye.

By increasing the degas time before deposition from one to ten minutes, the Ti content decreases to 7.2×10^{15} Ti-at/cm^2, and does not decrease further when increasing the degas time to 20 min [Fig. 9(b)]. Because minimal change in Ti uptake is observed from RBS measurements under conditions studied here, we utilize standard conditions of 6 s purges and 1 min degas for all depositions unless stated otherwise.

Using these conditions, we deposit various cycles of TiO_2 on each polymer (with and without PAG and before and after EUV exposure) to evaluate the potential for selective deposition. Surfaces are then analyzed with WCA to measure surface hydrophobicity and with RBS and XPS to measure Ti content, with results shown in Figs. 10, 11, and Table 3, respectively. Figure 10 shows WCA measurements taken after various TiO_2 cycle numbers to compare changes in surface hydrophobicity. For all unexposed polymers (both with and without PAG), the WCA decreases with increasing ALD cycle, corresponding to a decrease in hydrophobicity consistent with TiO_2 (WCA ~ 60 deg) depositing on the surface. After 100 cycles of ALD on PtBuMA, the contact angle dropped to $< \sim 30$ deg, consistent with the formation of a TiO_2 film on the polymer surface. For polymers with OH terminations (PHS and P(HS-r-MAA)), this decrease in WCA is already notable over the first 50 cycles, corresponding to a change in surface composition from polymer to TiO_2. The presence of PAG for these polymers results in a somewhat slower decrease in contact angle. When conducting ALD on these exposed polymers with PAG, the WCA decreases even more slowly. In contrast, PAG addition results in a more rapid decrease in WCA for PtBuMA. For the EUV-exposed PtBuMA, the WCA after exposure is already quite small (~ 35 deg), and therefore, does not change significantly during TiO_2 deposition.

Figure 11 shows the amount of deposited TiO_2 as measured by RBS as a function of the number of ALD cycles. For polymers without PAG, Ti content increases with increasing cycle

Fig. 11 RBS measurements of equivalent TiO_2 film thickness (left y-axis) calculated from Ti content (right y-axis) for various cycles of TiO_2 deposited from $TiCl_4$ and H_2O at 125°C on PtBuMA (blue squares), PHS (purple triangles), and P(HS-r-MAA) (pink circles) for samples of (a) polymers without PAG, (b) polymers with PAG, and (c) polymers with PAG after EUV exposure and PEB. Lines are drawn as guides to the eye. TiO_2 ALD on SiO_2 is included as black dashed line for reference.

Table 3 XPS measurements for the atomic concentration of C, O, Si, and Cl after 0, 50, and 100 cycles TiO$_2$ ALD on PtBuMA without PAG and PtBuMA with PAG and EUV exposure. Data are collected at an angle of 20 deg to the surface.

PtBuMA polymer	TiO$_2$ cycles	XPS atomic concentration				
		C 1s	O 1s	Si 2p	Ti 2p	Cl 2p
Unexposed	0	81.81	18.13	0.07	—	—
	50	52.01	34.30	0.39	13.03	0.27
	100	40.17	41.16	0.88	17.32	0.47
Exposed with PAG	0	83.99	15.49	0.53	—	—
	50	47.96	36.88	1.97	13.00	0.20
	100	39.53	41.55	1.05	17.2	0.68

number at a rate comparable to the expected TiO$_2$ growth rate on a SiO$_2$ surface (i.e., 0.037 nm/cycle), consistent with previous results.[8,9] The TiO$_2$ growth rate at 150°C on SiO$_2$ substrates is included in the figure for Ref. 23. This leads to ~4 nm TiO$_2$ deposited on each surface after 100 ALD cycles. Upon the addition of PAG, the TiO$_2$ growth per cycle (GPC) decreases somewhat for each film to ~0.025 nm/cycle. The same ~0.025 nm/cycle growth rate is observed on each polymer after EUV exposure, despite the difference in initial WCA on each surface (Figs. 6 and 10). These trends in Ti uptake are consistent with trends in WCA from Fig. 10. We note that because there was minimal change in surface chemistry (Figs. 4–5, Table 1) for the unexposed regions of these positive tone materials after development, TiO$_2$ deposition on EUV unexposed resist is expected to be similar before and after development. However, further investigations are needed to verify the effects of development of TiO$_2$ ALD on both exposed and unexposed regions, including the possible impact of resist scumming.

Table 3 shows the surface composition determined by XPS of the PtBuMA homopolymer and the EUV-exposed PtBuMA+PAG after various cycles of TiO$_2$ deposition. After 50 ALD cycles, the carbon concentration decreases from ~80 to ~50% on both samples, while the Ti and O concentrations increase to ~13% and ~35%, respectively. This is consistent with a TiO$_2$ film of approximately the same thickness being deposited on both polymer surfaces. Small amounts of Cl (<0.3%) are detected, which are attributed to residual Cl atoms in the film from the TiCl$_4$ precursor. After 100 ALD cycles, the concentration of C further decreases and the concentrations of Ti, O, and Cl further increase, again with approximately the same elemental concentrations on both the exposed and unexposed surfaces. Thus, XPS results support RBS measurements from Fig. 11. Overall, TiO$_2$ is successfully deposited on PtBuMA, PHS, and P(HS-r-MAA) polymers regardless of the presence of PAG or EUV exposure. This indicates that an etch-resistant TiO$_2$ layer could be successfully deposited on the remaining resist after development (in either a positive or negative tone process). If the underlying substrate inhibits TiO$_2$ growth (e.g., passivated SiO$_2$ or SiH), then this selective deposition will result in a hardened resist.

To evaluate how the TiCl$_4$ precursor initially reacts with the polymer surfaces during ALD, we verify the self-limiting nature of the surface reaction by repeating TiCl$_4$ doses either 1 or 10 times on the surface of P(HS-r-MAA) and perform RBS measurements to determine the resulting Ti content. In an ideal ALD process, once all available surface sites have reacted, no more material will be added to the surface. RBS results in Fig. 12 show that for P(HS-r-MAA) with or without PAG, and with or without EUV exposure, increasing the number of TiCl$_4$ doses produces approximately the same Ti content. This indicates that TiCl$_4$ reacts with all available surface OH sites and there is no significant TiCl$_4$ physisorption or sub-surface diffusion on these materials. We note that this self-limiting behavior of TiCl$_4$ may be different on different polymers, such as PtBuMA which does not have reactive OH sites on the surface.[9,30] These insights will be important to identifying causes of selectivity loss on polymers and developing strategies to inhibit TiO$_2$ growth on undesired regions. The exact mechanisms causing TiO$_2$ growth on
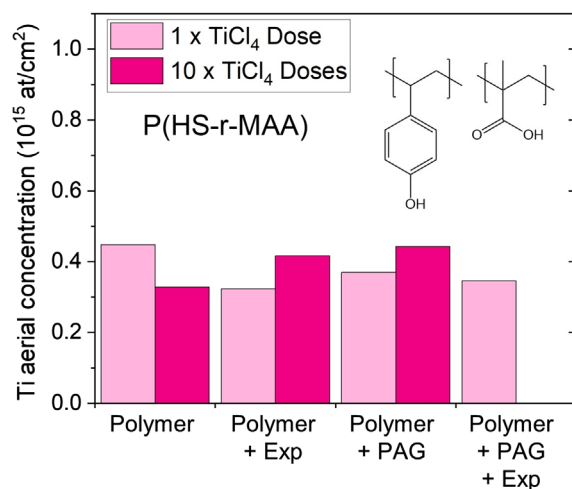
Fig. 12 RBS measurements of the Ti content after either one or ten $TiCl_4$ doses on P(HS-r-MAA) with and without PAG and before and after EUV exposure and PEB.

each polymer (in particular despite the hydrophobic starting surfaces) should be investigated in future work.

3.4 TiO_2 ALD on Polymers with Varied Protecting Groups

We next consider TiO_2 ALD on a methacrylate-based polymer with a different protecting group, specifically poly(cyclohexyl methacrylate) (PCHMA). Figure 13 shows RBS results during TiO_2 ALD at 125°C, with PtBuMA shown for reference. Interestingly, we observe a substantial delay in the TiO_2 deposition on this modified polymer material. Compared to the 0.029 nm/cycle GPC on PtBuMA, the initial growth rate on PCHMA is much smaller, yielding only ~0.5 nm TiO_2 after 100 cycles (compared with ~2.9 nm on PtBuMA or ~3.7 nm on SiO_2). This initial growth inhibition on PCHMA could be due to the bulkier protecting group or the different bonding structure compared to the polymers containing tBuMA and MAA. Using the definition of selectivity (S) in Eq. (1), where t represents the thickness on the growth (G, i.e., PCHMA) and nongrowth (NG, i.e., SiO_2 substrate) surfaces, respectively,[7] this result corresponds to a selectivity of ~76% after 100 cycles
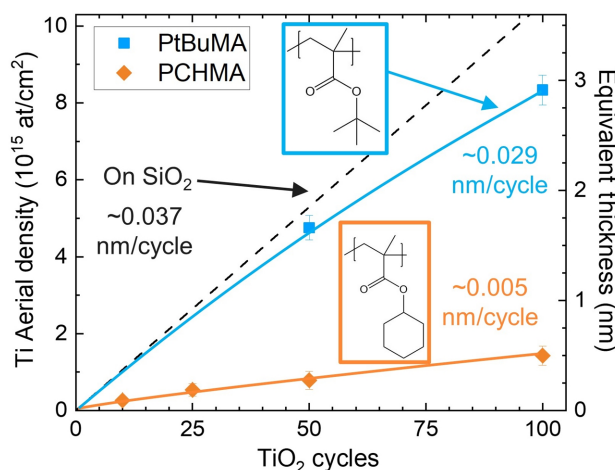
Fig. 13 RBS measurements of Ti content (left y-axis) and equivalent TiO_2 film thickness (right y-axis) for various cycles of TiO_2 deposited from $TiCl_4$ and H_2O at 125°C on PtBuMA (blue squares) and PCHMA (orange diamonds). Lines are drawn as guides to the eye. TiO_2 ALD on SiO_2 is included as black dashed line for reference.

$$S \cong \frac{t_G - t_{NG}}{t_G + t_{NG}}. \tag{1}$$

Thus, these results show that varying the resist structure is a viable way to induce selectivity during TiO_2 ALD. In this example, the structure of the PCHMA polymer shows promise for inhibiting deposition on a resist surface. For a positive-tone resist, this could be used for tone inversion either before development (deposition on exposed resist selective to unexposed resist) or after development (deposition on substrate selective to unexposed resist). Overall, the results presented here confirm the potential for ASD to be used successfully on thin polymers for EUV resist materials and are expected to be generally applicable to similar resist materials and deposited films. Additional work is needed to expand these results to thinner materials and different types of resists (e.g., by varying the CAR components or investigating nonchemically amplified resists), and to identify relevant selectivity loss mechanisms on resist materials.

4 Conclusion

We successfully demonstrate the compatibility of TiO_2 ASD with ~30 nm thin EUV resist materials. WCA and AFM measurements demonstrate thermal stability of PtBuMA, PHS, and P(HS-r-MAA) polymers at the operating temperature for TiO_2 ALD (i.e., 125°C). We emphasize the importance of characterizing resist materials with all required resist components (e.g., with PAG and EUV exposure), as these factors have important impacts on resist surface properties and thermal stability for ASD. TiO_2 is successfully deposited on each of these polymers with and without PAG and before and after EUV exposure. Thus, these polymers are promising candidates for resist-hardening applications performed after development on a substrate that inhibits TiO_2 deposition. On the other hand, TiO_2 deposition on PCHMA is inhibited for the first 100 ALD cycles, making this an interesting option for tone inversion applications. We achieve 76% selectivity after 100 ALD cycles on PCHMA relative to the SiO_2 substrate, resulting in a TiO_2 film of ~3.7 nm on SiO_2. Thus, we conclude that TiO_2 ASD is compatible with organic EUV resist processing, and we furthermore demonstrate the successful selectivity of TiO_2 between different types of polymers. Future work is needed to expand TiO_2 ASD to additional polymers, copolymers, and to elucidate the resist characteristics that enable or inhibit TiO_2 ALD, including the effects of common resist additives such as photo decomposable bases, underlayers, and development. Additionally, further investigation is needed to expand these results to patterned substrates with various critical dimensions, thereby elucidating the effects of pattern dimensions, edge effects, stochastics, and partial exposure on selectivity.

Acknowledgments

References

1. L. Li et al., "Extreme ultraviolet resist materials for sub-7 nm patterning," *Chem. Soc. Rev.* **46**, 4855–4866 (2017).
2. C. D. Higgins et al., "Resolution, line-edge roughness, sensitivity tradeoff, and quantum yield of high photo acid generator resists for extreme ultraviolet lithography," *Jpn. J. Appl. Phys.* **50**, 036504 (2011).
3. N. Mojarad, J. Gobrecht, and Y. Ekinci, "Beyond EUV lithography: a comparative study of efficient photoresists' performance," *Sci. Rep.* **5**, 9235 (2015).
4. T. Fujimori, T. Tsuchihashi, and T. Itani, "Recent progress of negative-tone imaging process and materials with EUV exposure," *Proc. SPIE* **9425**, 942505 (2015).

5. C. Sixt, "Surface functionalisation of extreme ultraviolet photoresist material for area-selective deposition," MS Thesis, KU Leuven (2019).

6. H. Tsubaki et al., "Negative-tone imaging with EUV exposure toward 13 nm hp," *Proc. SPIE* **9776**, 977608 (2016).

7. G. N. Parsons and R. D. Clark, "Area-selective deposition: fundamentals, applications, and future outlook," *Chem. Mater.* **32**(12), 4920–4953 (2020).

8. S. K. Song, H. Saare, and G. N. Parsons, "Integrated isothermal atomic layer deposition/atomic layer etching supercycles for area-selective deposition of TiO_2," *Chem. Mater.* **31**(13), 4793–4804 (2019).

9. A. Sinha, D. W. Hess, and C. L. Henderson, "Area selective atomic layer deposition of titanium dioxide: effect of precursor chemistry," *J. Vac. Sci. Technol. B* **24**(6), 2523 (2006).

10. F. Grillo et al., "Area-selective deposition of ruthenium by area-dependent surface diffusion," *Chem. Mater.* **32**(22), 9560–9572 (2020).

11. R. A. Nye et al., "In situ analysis of growth rate evolution during molecular layer deposition of ultra-thin polyurea films using aliphatic and aromatic precursors," *Dalton Trans.* **51**(5), 1838–1849 (2022).

12. R. A. Nye et al., "Understanding molecular layer deposition growth mechanisms in polyurea via picosecond acoustics analysis," *Chem. Mater.* **32**(4), 1553–1563 (2020).

13. J.-S. Kim and G. N. Parsons, "Nanopatterned area-selective vapor deposition of PEDOT on SiO_2 vs Si-H: improved selectivity using chemical vapor deposition vs molecular layer deposition," *Chem. Mater.* **33**(23), 9221–9230 (2021).

14. R. Clark et al., "Perspective: new process technologies required for future devices and scaling," *APL Mater.* **6**(5), 058203 (2018).

15. J. Soethoudt et al., "Insight into selective surface reactions of dimethylamino-trimethylsilane for area-selective deposition of metal, nitride, and oxide," *J. Phys. Chem. C* **124**(13), 7163–7173 (2020).

16. R. Wojtecki et al., "Additive lithography–organic monolayer patterning coupled with an area-selective deposition," *ACS Appl. Mater. Interfaces* **13**(7), 9081–9090 (2021).

17. K. Van Dongen, D. De Simone, and A. Delabie, "Surface passivation using aminosilanes for area-selective atomic layer deposition and extreme ultraviolet lithography," MS Thesis, KU Leuven (2020).

18. H. Yao et al., "Spin-on metal oxides and their applications for next generation lithography," *J. Photopolym. Sci. Technol.* **29**(1), 59–67 (2016).

19. R. A. Nye et al., "Improving polymethacrylate EUV resists with TiO_2 area-selective deposition," *Proc. SPIE* **12055**, 120550C (2022).

20. M. H. Park et al., "Selective atomic layer deposition of titanium oxide on patterned self-assembled monolayers formed by microcontact printing," *Langmuir* **20**(6), 2257–2260 (2004).

21. L. Lecordier, S. Herregods, and S. Armini, "Vapor-deposited octadecanethiol masking layer on copper to enable area selective Hf_3N_4 atomic layer deposition on dielectrics studied by in situ spectroscopic ellipsometry," *J. Vac. Sci. Technol. A* **36**(3), 031605 (2018).

22. E. Stevens et al., "Area-selective atomic layer deposition of TiN, TiO_2, and HfO_2 on silicon nitride with inhibition on amorphous carbon," *Chem. Mater.* **30**, 3223–3232 (2018).

23. R. A. Nye et al., "Mechanisms for undesired nucleation on H-terminated Si and dimethylamino-trimethylsilane passivated SiO_2 during TiO_2 area-selective atomic layer deposition," *Appl. Phys. Lett.* **121**(8), 082102 (2022).

24. A. Sinha, D. W. Hess, and C. L. Henderson, "A top surface imaging method using area selective ALD on chemically amplified polymer photoresist films," *Electrochem. Solid-State Lett.* **9**(11), G330–G333 (2006).

25. H. Saare et al., "Effect of reactant dosing on selectivity during area-selective deposition of TiO_2 via integrated atomic layer deposition and atomic layer etching," *J. Appl. Phys.* **128**(10), 105302 (2020).

26. G. N. Parsons, "Atomic layer deposition on soft materials," in *Atomic Layer Deposition of Nanostructured Materials*, N. Pinna and M. Knez, Eds., pp. 271–300, John Wiley & Sons, Ltd. (2012).

27. G. N. Parsons et al., "Mechanisms and reactions during atomic layer deposition on polymers," *Coord. Chem. Rev.* **257**, 3323–3331 (2013).
28. A. H. Brozena, C. J. Oldham, and G. N. Parsons, "Atomic layer deposition on polymer fibers and fabrics for multifunctional and electronic textiles," *J. Vac. Sci. Technol. A* **34**(1), 010801 (2016).
29. C. A. Wilson, R. K. Grubbs, and S. M. George, "Nucleation and growth during Al_2O_3 atomic layer deposition on polymers," *Chem. Mater.* **17**, 5625–5634 (2005).
30. A. Sinha, D. W. Hess, and C. L. Henderson, "Transport behavior of atomic layer deposition precursors through polymer masking layers: influence on area selective atomic layer deposition," *J. Vac. Sci. Technol. B: Microelectron. Nanometer Struct.* **25**(5), 1721 (2007).

Rachel A. Nye is a PhD candidate at North Carolina State University. She received her BS degree in chemistry and Spanish from Washington & Jefferson College in 2017, and her MS and PhD degrees in chemical engineering from North Carolina State University in 2019 and 2022, respectively. She is the author of three journal papers and two conference proceedings. Her current research interests include thin film deposition and characterization, area-selective deposition, and organic thin films.

Kaat Van Dongen received her bachelor's and master's degrees in chemistry from KU Leuven in 2018 and 2020, respectively. She is a PhD student at KU Leuven and Imec. Her main research fields are area-selective deposition specifically through surface de-activation and thin-film deposition.

Gregory N. Parsons explores atomic-scale synthesis and processing of advanced electronic and thin-film materials. He joined the faculty of the Chemical and Biomolecular Engineering Department at North Carolina State University in 1992, and since then, he has supported, advised, and graduated more than 40 PhD students, including leaders in academia, national laboratories, and industrial research and practice.

Annelies Delabie is a professor in the Faculty of Science at the University of Leuven (KU Leuven) in Belgium and a principal member of technical staff at imec, research institute for nano-electronics and digital technologies in Belgium. She received her MS degree in chemistry and PhD in science from the University of Leuven in 1997 and 2001, respectively. She is the author of more than 200 scientific publications and 10 patents. Her current research interests include atomic layer deposition, chemical vapor deposition, area-selective deposition, and EUV lithography.

Biographies of the other authors are not available.